Supplementary Materials for

Coherent imaging spectroscopy of a quantum many-body spin system

C. Senko,* J. Smith, P. Richerme, A. Lee, W. C. Campbell, C. Monroe

*Corresponding author. E-mail: csenko@umd.edu

Published 25 July 2014, *Science* **345**, 430 (2014)
DOI: 10.1126/science.1251422

This PDF file includes:

Supplementary Materials: Coherent Imaging Spectroscopy of a Quantum Many-Body Spin System

C. Senko[1,*], J. Smith[1], P. Richerme[1], A. Lee[1],
W. C. Campbell[2], and C. Monroe[1]

[1]Joint Quantum Institute, University of Maryland Dept. of Physics and
National Institute of Standards and Technology, College Park, MD 20742, USA
[2]Department of Physics and Astronomy, University of California, Los Angeles, CA 90095

[*]To whom correspondence should be addressed; E-mail: csenko@umd.edu

Spin-spin couplings

The spin-spin couplings described in Eq. 1 result from applying a spin-dependent optical dipole force in the σ^x basis with the Raman lasers. The wavevector difference Δk of the two laser beam paths is along one of the principal transverse axes of the trap, allowing the lasers to couple to the collective motional modes and virtually excite phonons that mediate the spin-spin interaction. A pair of beat frequencies are symmetrically detuned from the resonant transition between the spin states, at $\nu_0 = 12.642819$ GHz, by an amount μ which is of the same order as the motional mode frequencies. In the Lamb-Dicke regime, this generates a Mølmer-Sørensen-type interaction (*33*) given by

$$H_{MS} = \sum_{i,m=1}^{N} \eta_{i,m}\Omega_i \sin(2\pi\mu t)\sigma_i^x \left[\hat{a}_m e^{-2\pi i\nu_m t} + \hat{a}_m^\dagger e^{2\pi i\nu_m t}\right]. \tag{S1}$$

Here, i and m index the ions and motional modes, respectively; Ω_i represents the equivalent resonant carrier Rabi frequency at ion i, ν_m the frequency of the mth collective mode

of motion, $\hat{a}_m$ ($\hat{a}_m^\dagger$) the annihilation (creation) operator for mode m, $\eta_{i,m} = b_{i,m}\frac{\Delta k}{2\pi}\sqrt{\frac{h}{2M\nu_m}}$ is the Lamb-Dicke factor, coupling ion i to mode m, $b_{i,m}$ is the normal mode matrix and M is the mass of a single $^{171}\mathrm{Yb}^+$ ion (*34*).

In the limit of a large detuning, $|\mu - \nu| \gg \eta_{i,m}\Omega$, the motion is only virtually excited and the effective Hamiltonian is the spin-spin interaction,

$$H = \sum_{i<j} J_{i,j}\sigma_i^x\sigma_j^x. \tag{S2}$$

Here the spin-spin couplings are given by (*14*)

$$J_{i,j} = \Omega_i\Omega_j\Omega_R\sum_{m=1}^{N}\frac{b_{i,m}b_{j,m}}{\mu^2 - \nu_m^2}, \tag{S3}$$

where $\Omega_R = \frac{h(\Delta k/2\pi)^2}{2M}$ is the recoil frequency. We note that for the experiments reported here, the detuning from the center-of-mass mode $\mu - \nu_1$ was between $3\eta\Omega$ and $4\eta\Omega$, where η is the Lamb-Dicke factor for the COM mode (which is the highest in frequency of the transverse modes), and Ω is assumed to be uniform for each ion. Thus, excitation of the COM mode is less than 10% (and excitation of the other modes is even lower).

The frequencies and eigenvectors of the transverse motional modes used above can be fully characterized (in the limit where the trapping potential can be well approximated by a 3-dimensional harmonic oscillator) by the secular frequencies characterizing the potential in the x transverse direction and the z axial direction (*34*). For the experiments reported in this work, the transverse trapping frequency is roughly ν_1 =4.8 MHz and the axial trapping frequency is varied between 0.59 MHz – 1.05 MHz.

When the beatnote is tuned to $\mu > \nu_1$, the interaction profile varies between a uniform all-to-all coupling ($J_{i,j} \sim J_0$) in the limit where the μ is close enough to ν_1 to neglect contributions from other modes, to a dipolar falloff ($J_{i,j} \sim J_0/|i-j|^3$) in the limit where μ is far detuned from all the modes. In between these limits, numerical calculations

show that the interaction profiles can be roughly approximated by $J_{i,j} \sim J_0/|i-j|^\alpha$ with $0 < \alpha < 3$. The exponent α depends on the relative detunings from all the modes, and can be varied either by changing μ or by changing the axial trap frequency.

In our experiments, the main causes of drifts in the Hamiltonian are due to laser intensity noise (e.g., from pointing instability), which directly affects Ω_i, and to drifts in the transverse trap frequency ν_x^{COM} (e.g., due to slight internal temperature changes in the resonator delivering RF voltage to the trap), which affects all the mode frequencies ν_m and hence the detunings $\mu - \nu_m$.

Measurement of spin states

The detection cycle for each experiment consists of exposing the ions to 'detection' light, resonant with the $|\uparrow\rangle_z$ ('bright') state but not the $|\downarrow\rangle_z$ ('dark') state, for 3 ms. An objective with a numerical aperture of NA=0.23 collects the resulting fluorescence, which is imaged onto an intensified CCD camera. To calibrate the readout, we perform 1000 cycles of preparing and measuring an all-dark state, $|\downarrow\downarrow\downarrow\cdots\rangle_z$, and 1000 cycles of an all-bright state, $|\uparrow\uparrow\uparrow\cdots\rangle_z$. Single-shot discrimination is performed by summing the columns of the resulting image into a 1-dimensional row, since the vertical direction yields no additional information in a linear chain, and fitting the resulting profile to a sum of Gaussians whose positions and widths are determined from the calibration images. The individual ion states are then discriminated by comparing the fit amplitudes to calibrated thresholds (see below).

The calibration also allows us to determine the detection errors for each ion, i.e. the probability of misdiagnosing a dark state as bright or vice versa for a given threshold. These known errors are used to correct the probability distributions for detection errors, while also considering standard errors from shot noise (*35*).

The optimal thresholds are determined by performing a Monte Carlo simulation in which certain target states are 'prepared' by randomly choosing an amplitude from the appropriate calibration ensemble (e.g., for the target state $|1010\cdots\rangle$ the amplitude of the first ion is chosen from the pool of amplitudes which were fit to the first ion in the bright calibration), discriminated with a given threshold, and corrected for the detection error given the chosen threshold. A threshold is then chosen that is insensitive to statistical fluctuations and gives corrected probability distributions that match the known input ensemble well; the recovered probability distributions are nearly identical for a wide range of threshold choices.

Measurement of energy splittings

In the weak-field regime, we know that the only states that are coupled are those which differ by a single spin flip. Thus, for a given input state, we know exactly which states can be reached by the modulated transverse field (e.g., from $|111\cdots11\rangle$ the only states which are coupled to first order are $|011\cdots11\rangle$, $|101\cdots11\rangle$, $\cdots$, $|111\cdots10\rangle$). For each frequency scan, we extract the population of each coupled state as a function of modulation frequency. These data sets are expected to show a peak at the actual energy splitting.

We fit Lorentzian functions to these peaks to determine each energy splitting:

$$L(x, x_0, w, A, o) = A\frac{w^2}{(x - x_0)^2 + w^2} + o, \tag{S4}$$

where the offset o is included because in some cases the baseline population of a final state may be nonzero due to, e.g., off-resonant coupling during the first excitation pulse. The center frequency, x_0, thus determined is a direct measure of the energy splitting between the initial and final states. (Nearly identical results are obtained using a functional form of $A\ \mathrm{sech}\frac{x-x_0}{w} + o$ or $A\ \mathrm{sinc}^2\frac{x-x_0}{w} + o$ to fit the peaks.) In some cases, especially when multiple sequential excitations are performed, there may be insufficient population

transfer to discern a peak above the noise floor. In most cases, there will be questions of how to choose the best fit out of multiple possible fits, or whether any of the possible fits are plausible. We will now describe our method for identifying the best fit, or the absence of a good fit.

Seeding the fitting routine

We perform our fits in Mathematica using the NonlinearModelFit function. This function allows us to input a data set, a fit function, a set of weights corresponding to the measurement errors, and an initial guess for the fitting parameters, and can return parameter standard errors in addition to best fit parameters. As with most fitting routines, it is sensitive to the initial guess for the center value x_0, and seeding the routine with different values will return different guesses for the peak location. We therefore compare multiple fits seeded with different initial guesses. For each data set, we calculate the mean and standard deviation of the y values. Then, we select all of the points whose y value is more than 1.5 standard deviations away from the mean, and use the x values of these points as seeds to the fitting routine.

Identifying a bad fit

Some of the fits will be immediately implausible. E.g., since the y axis is a probability, the amplitude of the Lorentzian should never exceed 1. We use several such criteria, where a fit is considered "good" only if it meets all of the following conditions:

- $0 < A < 1$ eliminates those fits where an unphysical probability occurs. (Typically this is only violated when the fitter finds a local optimum in a spuriously narrow peak with an amplitude many orders of magnitude larger than 1.)
- $w < 0.6$ kHz eliminates fits which key in on a slow variation in the background level.

For a 3 ms pulse (of a strength which drives less than a π pulse on resonance), each peak is expected to be roughly 0.15 kHz wide (based on both numerical evolution of the Schrodinger equation in our many-body system, and on the Rabi solution for driving an isolated two-level system), so this leaves a large margin for typical variation in the widths.

- $w > \Delta w/2$, where Δw is the standard error on the fit parameter, eliminates a few fits which key in on two neighboring points that are slightly higher than the nearby points but still within the noise, resulting in an implausibly tall and narrow peak (which nevertheless tends to have $A < 1$); such fits typically have a large Δw.

- $A > 1.5\ S$, where S is the mean shot noise for the data set being fit, imposes the requirement that the signal-to-noise ratio be at least 1.5.

These criteria, as with any criteria for discriminating good fits from bad, are necessarily subjective, and are chosen to be reasonably permissive of plausible fits to noisy data while still eliminating those fits which are blatantly bad on visual inspection, e.g., they successfully eliminate all fits to those data sets which visually appear most consistent with a (noisy) flat line. Of the remaining fits, should there be multiple good fits with different x_0 seeds for a single data set, the fit with the highest R^2 is chosen for the remaining analyses.

Measuring coupling profiles

For each coupling profile, frequency scans are performed with initial states of $|11111111\rangle$ and all single-defect states thereof, i.e. $|01111111\rangle$, $\cdots$, $|11111110\rangle$. The single-defect states are prepared with a pulse of the modulated transverse field. Using the methods described above, we extract all of the measurable energy splittings. For each energy

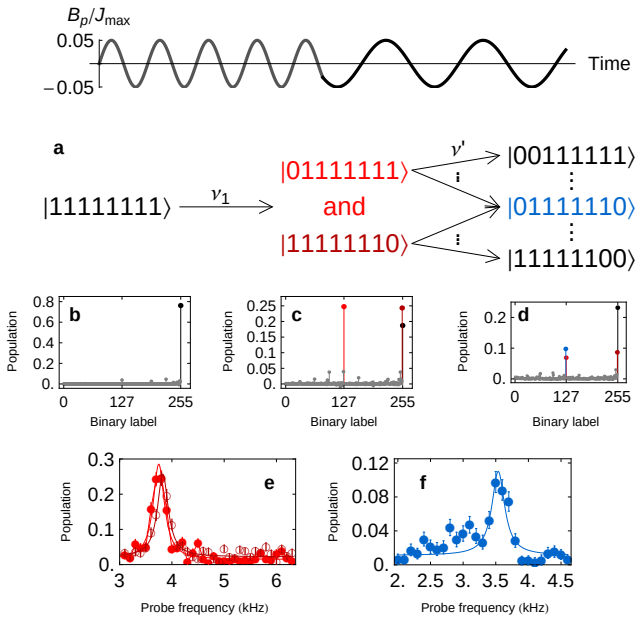

Figure S1: (a): Sketch of protocol for driving sequential excitations. (b)-(d): plots of the measured populations in each of the 2^N states in a system of $N = 8$ spins. We apply sequential pulses of the modulated transverse field to an initial polarized state, shown in (b). The first pulse drives transitions into states with single defects, $|01111111\rangle$ and $|11111110\rangle$ (c), and the second pulse can then create states with two defects (d). (e): Population in either of the states with a single defect on the end vs. the frequency of the first pulse. (f): Fixing the first pulse on resonance from (e), we show the population of a state with two defects, $|01111110\rangle$, vs. the frequency of the second pulse.

Trace over 1?	Trace over 2?	Trace over 3?	Trace over 4?	$\langle W_{ss} \rangle$	Number ions involved, N	$\langle W_{ss} \rangle_{\min}$
No	No	No	No	-1.62(22)	4	-3
Yes	No	No	No	-0.382(121)	3	-2
No	Yes	No	No	-0.847(96)	3	-2
No	No	Yes	No	-0.735(101)	3	-2
No	No	No	Yes	-0.300(114)	3	-2
Yes	Yes	No	No	-0.115(40)	2	-1
Yes	No	Yes	No	-0.111(41)	2	-1
Yes	No	No	Yes	-0.001(44)	2	-1
No	Yes	Yes	No	-0.279(37)	2	-1
No	Yes	No	Yes	-0.081(38)	2	-1
No	No	Yes	Yes	-0.055(39)	2	-1

Table S1: Measured values of the spin-squeezing-type witness W_{ss} described in the text, compared to theoretical values for a perfect 4-spin state $|\Psi_W\rangle$ (rightmost column); a negative value certifies that the state is nonseparable and hence that at least two of the spins are entangled. By tracing over individual spins, we see that all pairs except ions 2 and 3 are at least 1σ below zero, showing that these pairs are entangled; entanglement between each possible pair is consistent with the multipartite entanglement that would be expected for a perfect W state.

splitting, we know the initial and final spin ordering and so know how to relate the energy difference to the spin-spin couplings, as described in the main text. We use these relations to build a design matrix $\mathbf{A}$ and a response vector $\vec{y}$ such that $\mathbf{A}.\vec{x} = \vec{y}$, where $\vec{y}$ is a vector consisting of the measured energy splittings, $\vec{x}$ is a vector consisting of the spin-spin couplings, and $\mathbf{A}$ is a matrix with rank equal to or greater than the number of independent couplings (i.e., $\mathbf{A}$ has $\binom{N}{2}$ columns corresponding to the $\binom{N}{2}$ couplings, and *at least* $\binom{N}{2}$ independent rows). Mathematica's LinearModelFit routine is then used to perform a linear least-squares analysis determining which vector $\vec{x}$ minimizes the sum of squares of residuals, $\min |\mathbf{A}\vec{x} - \vec{y}|$. Additionally, the data points (i.e. energy splittings) are weighted according to $1/\sigma_{x_0}$, where σ_{x_0} is the estimated error in the fit center x_0 that was used to determine each splitting. As a side note, we have taken advantage of the knowledge that our couplings are roughly of the form J_0/r^α (and in particular, all share

the same sign), which means that single-defect states will always be lower energy than the polarized state in our system, and (for the systems presented here) two-defect states are lower in energy than single-defect states. Without this knowledge it would be necessary to determine not only the magnitude of the energy splittings, as we do here, but also the sign, in order to fully constrain the coupling matrix. This is however achievable by making a second set of measurements with a known longitudinal field $B_x \sum_{i=1}^{N} \sigma_i^x$, which will shift the energies in a known direction. Comparison between the two data sets to determine whether B_x shifts the levels closer together or further apart would yield the sign of the energy splitting.

Scalability considerations for characterizing power-law-like interaction profiles

It is important to consider how well our technique will scale to larger systems. Characterizing all NxN interactions among N spins requires $N+1$ scans using the method we describe in the text. However, the various energy splittings may become more closely spaced for large systems, and hence the interaction time per scan will also depend on the system size. Here we estimate the interaction time necessary to resolve the most closely spaced energy splittings in a system with homogeneous power-law interactions,

$$H = \sum_{i,j} J_{i,j} \sigma_i^x \sigma_j^x \tag{S5}$$

$$J_{i,j} = \frac{J_0}{|i-j|^\alpha}, \tag{S6}$$

assuming that the system starts in the $|{\downarrow\downarrow}\cdots{\downarrow}\rangle_x$ state. In this case, the energy required to flip the ith spin from the end of an N spin chain is:

$$E_i = 2\left(\sum_{k=1}^{i-1} J_{i,k} + \sum_{k=i+1}^{N} J_{i,k}\right) = 2J_0\left(\sum_{k=1}^{i-1} \frac{1}{k^\alpha} + \sum_{k=1}^{N-i} \frac{1}{k^\alpha}\right). \tag{S7}$$

The energy cost is lowest for flipping the spin on the end. In this case, the energy is simply 2×(nearest neighbor coupling + next nearest neighbor coupling + ...) = 2 $(1+1/2^\alpha+1/3^\alpha+\cdots+1/(N-1)^\alpha)$. For flipping the second spin, the contribution of the final coupling $J_{1,N}=1/(N-1)^\alpha$ is replaced by another nearest neighbor contribution, as we now have $2(J_{1,2}+J_{2,3}+J_{2,4}+...+J_{2,N})=2(1+1+1/2^\alpha+...+1/(N-2)^\alpha)$. Since $1\geq 1/(N-1)^\alpha$ for our limitation of $0<\alpha<3$, it will always cost more energy to flip the second spin than the first. By induction, we can see that due to the monotonic falloff of the couplings, it will always cost more energy to flip a spin closer to the center than a spin closer to the edge.

The energy of flipping spin i monotonically increases with i ($1\leq i\leq N/2$). However, to estimate the interaction time necessary to resolve neighboring energy splittings, we must estimate the spacing between these energy splittings. From Eq. S7, this is:

$$E_i-E_{i-1}\equiv\Delta_i=2J_0\left(\frac{1}{(i-1)^\alpha}-\frac{1}{(N-i+1)^\alpha}\right). \tag{S8}$$

One can show that $|\Delta_i|=0$ at $i=N/2+1$, which intuitively makes sense for even N since the energy of flipping either of the middle two spins should be the same. Furthermore, the derivative is negative:

$$\frac{d\Delta_i}{di}=-2J_0\alpha\left(\frac{1}{(i-1)^{\alpha+1}}+\frac{1}{(N-i+1)^{\alpha+1}}\right), \tag{S9}$$

so the two (nondegenerate) resonances which will be closest together are those with $i=N/2$ and $i=N/2-1$. In this case,

$$\Delta_{N/2}=2J_0\left(\frac{1}{(N/2-1)^\alpha}-\frac{1}{(N/2+1)^\alpha}\right), \tag{S10}$$

which can be rearranged as

$$\Delta_{N/2}=2J_0\left(\frac{2}{N}\right)^\alpha\left(\frac{1}{(1-\frac{2}{N})^\alpha}-\frac{1}{(1+\frac{2}{N})^\alpha}\right), \tag{S11}$$

or, for large N,

$$\Delta_{N/2} \approx 8J_0 \left(\frac{2}{N}\right)^{\alpha} \frac{\alpha}{N}. \tag{S12}$$

We therefore see that the smallest energy splitting scales like $1/N^{\alpha+1}$, which sets the scale for the frequency resolution necessary to excite individual resonances (as opposed to driving multiple resonances simultaneously). This means that the necessary interaction time for resolving the energies scales like $1/\Delta_{N/2} \sim N^{\alpha+1}/J_0$. Thus, the total time necessary to perform N frequency scans will scale polynomially as $N^{\alpha+2}$. This is a conservative estimate; adaptive techniques which increase the interaction time only in regions of high energy state density could decrease the total time necessary to characterize the entire system.

For smaller systems, Eq. S11 can be used to estimate this characterization time quantitatively – for example, comparing the 8 spin system characterized experimentally to a 30 spin system, which is sufficiently large that numerical simulation of its dynamics will be infeasible. Typical values for the coupling profile might be $J_0 = 1$ kHz and $\alpha = 1$, for which the necessary probe time $1/\Delta_{N/2}$ to fully resolve neighboring eigenstates is roughly 4 ms in an 8 spin system or 50 ms in a 30 spin system. In the absence of factors such as background gas collisions that limit the experimental repetition rate, this means an 8 spin system could be fully characterized in roughly an hour (assuming (A) only 5 frequency scans are required due to left-right symmetry considerations, (B) each scan probes 50 frequencies, and (C) 1000 repetitions of each experiment are performed). A similar calculation for a 30 spin system leads to an estimate of 22 hours, still less than a day. We note that the tactic of resolving each energy level negates the need to perform more repetitions of each experiment to decrease quantum projection noise; so long as the initial state can be created with sufficient fidelity, the population driven into the state of interest should be the same regardless of the number of spins.

This estimate can be compared to alternative techniques, such as that demonstrated in (*27*), where each pair is addressed separately to directly measure its coupling strength. There, the idea is to initialize all ions other than the pair of interest into an auxiliary state that does not participate in the spin dynamics, then characterize the frequency of oscillation between e.g. $|{\downarrow}{\uparrow}\rangle$ and $|{\uparrow}{\downarrow}\rangle$. To accurately estimate a frequency J in this manner, the system must be allowed to evolve for a time of at least $1/J$, so the longest interaction time will be given by $1/J_{1,N} = (N-1)^{\alpha}/J_0$. To characterize $N(N-1)/2$ interactions will therefore take a total time of order $N(N-1)^{\alpha+1}/J_0$, leading to the same scaling behavior of $N^{\alpha+2}/J_0$. Thus, though our method shows similar scaling behavior in this analysis, it still compares favorably due to the lack of overhead for individual addressing. Additionally, the method in (*27*) will need to probe each pair for varying lengths of time in order to reliably estimate the frequency of oscillation in the time evolution, so it will have a larger constant prefactor associated with the scaling behavior. For these reasons, spectroscopic methods for characterizing fully connected spin systems are a useful and scalable addition to the toolbox of verification techniques.

References

1. J. I. Cirac, P. Zoller, Goals and opportunities in quantum simulation. *Nat. Phys.* **8**, 264–266 (2012). doi:10.1038/nphys2275

2. B. A. Cipra, The Ising model is NP-complete. *SIAM News* **33** (6), 654 (2000); www.siam.org/pdf/news/654.pdf.

3. E. Schneidman, M. J. Berry 2nd, R. Segev, W. Bialek, Weak pairwise correlations imply strongly correlated network states in a neural population. *Nature* **440**, 1007–1012 (2006). Medline doi:10.1038/nature04701

4. S. Liu, L. Ying, S. Shakkottai, in *48th Annual Allerton Conference on Communication, Control, and Computing* (IEEE, New York, 2010), pp. 570–576. doi:10.1109/ALLERTON.2010.5706958.

5. H. T. Diep, Ed., *Frustrated Spin Systems* (World Scientific, Singapore, 2005).

6. R. Feynman, Simulating physics with computers. *Int. J. Theor. Phys.* **21**, 467–488 (1982). doi:10.1007/BF02650179

7. S. Lloyd, Universal quantum simulators. *Science* **273**, 1073–1078 (1996). Medline doi:10.1126/science.273.5278.1073

8. *Nature Physics*, Insight Issue: "Quantum Simulation" **8**, 264 (2012).

9. A. Aspuru-Guzik, P. Walther, Photonic quantum simulators. *Nat. Phys.* **8**, 285–291 (2012). doi:10.1038/nphys2253

10. R. Blatt, C. F. Roos, Quantum simulations with trapped ions. *Nat. Phys.* **8**, 277–284 (2012). doi:10.1038/nphys2252

11. I. Bloch, J. Dalibard, S. Nascimbene, Quantum simulations with ultracold quantum gases. *Nat. Phys.* **8**, 267–276 (2012). doi:10.1038/nphys2259

12. P. Hauke, F. M. Cucchietti, L. Tagliacozzo, I. Deutsch, M. Lewenstein, Can one trust quantum simulators? *Rep. Prog. Phys.* **75**, 082401 (2012). Medline doi:10.1088/0034-4885/75/8/082401

13. D. Porras, J. I. Cirac, Effective quantum spin systems with trapped ions. *Phys. Rev. Lett.* **92**, 207901 (2004). Medline doi:10.1103/PhysRevLett.92.207901

14. K. Kim, M. S. Chang, R. Islam, S. Korenblit, L. M. Duan, C. Monroe, Entanglement and tunable spin-spin couplings between trapped ions using multiple transverse modes. *Phys. Rev. Lett.* **103**, 120502 (2009). Medline doi:10.1103/PhysRevLett.103.120502

15. K. Kim, M. S. Chang, S. Korenblit, R. Islam, E. E. Edwards, J. K. Freericks, G. D. Lin, L. M. Duan, C. Monroe, Quantum simulation of frustrated Ising spins with trapped ions. *Nature* **465**, 590–593 (2010). Medline doi:10.1038/nature09071

16. R. Islam, E. E. Edwards, K. Kim, S. Korenblit, C. Noh, H. Carmichael, G. D. Lin, L. M. Duan, C. C. Wang, J. K. Freericks, C. Monroe, Onset of a quantum phase transition with a trapped ion quantum simulator. *Nat. Commun.* **2**, 377 (2011). Medline doi:10.1038/ncomms1374

17. J. W. Britton, B. C. Sawyer, A. C. Keith, C. C. Wang, J. K. Freericks, H. Uys, M. J. Biercuk, J. J. Bollinger, Engineered two-dimensional Ising interactions in a trapped-ion quantum simulator with hundreds of spins. *Nature* **484**, 489–492 (2012). Medline doi:10.1038/nature10981

18. R. Islam, C. Senko, W. C. Campbell, S. Korenblit, J. Smith, A. Lee, E. E. Edwards, C. C. Wang, J. K. Freericks, C. Monroe, Emergence and frustration of magnetism with variable-range interactions in a quantum simulator. *Science* **340**, 583–587 (2013). Medline doi:10.1126/science.1232296

19. P. Richerme, C. Senko, J. Smith, A. Lee, S. Korenblit, C. Monroe, Experimental performance of a quantum simulator: Optimizing adiabatic evolution and identifying many-body ground states. *Phys. Rev. A* **88**, 012334 (2013). doi:10.1103/PhysRevA.88.012334

20. Materials and methods are available as supplementary material on *Science* Online.

21. J. Schachenmayer, B. P. Lanyon, C. F. Roos, A. J. Daley, Entanglement growth in quench dynamics with variable range interactions. *Phys. Rev. X* **3**, 031015 (2013). 10.1103/PhysRevX.3.031015

22. P. Hauke, L. Tagliacozzo, Spread of correlations in long-range interacting quantum systems. *Phys. Rev. Lett.* **111**, 207202 (2013). Medline doi:10.1103/PhysRevLett.111.207202

23. M. van den Worm, B. C. Sawyer, J. J. Bollinger, M. Kastner, Relaxation timescales and decay of correlations in a long-range interacting quantum simulator. *New J. Phys.* **15**, 083007 (2013). doi:10.1088/1367-2630/15/8/083007

24. Z.-X. Gong, L.-M. Duan, Prethermalization and dynamic phase transition in an isolated trapped ion spin chain. *New J. Phys.* **15**, 113051 (2013). doi:10.1088/1367-2630/15/11/113051

25. M. Knap, A. Kantian, T. Giamarchi, I. Bloch, M. D. Lukin, E. Demler, Probing real-space and time-resolved correlation functions with many-body Ramsey interferometry. *Phys. Rev. Lett.* **111**, 147205 (2013). Medline doi:10.1103/PhysRevLett.111.147205

26. A. Khromova, Ch. Piltz, B. Scharfenberger, T. F. Gloger, M. Johanning, A. F. Varón, Ch. Wunderlich, Designer spin pseudomolecule implemented with trapped ions in a magnetic gradient. *Phys. Rev. Lett.* **108**, 220502 (2012). Medline doi:10.1103/PhysRevLett.108.220502

27. P. Jurcevic, B. P. Lanyon, P. Hauke, C. Hempel, P. Zoller, R. Blatt, C. F. Roos, Quasiparticle engineering and entanglement propagation in a quantum many-body system, *Nature* **511**, 202–205 (2014). doi:10.1038/nature13461

28. S. Olmschenk, K. Younge, D. Moehring, D. Matsukevich, P. Maunz, C. Monroe, Manipulation and detection of a trapped Yb^+ hyperfine qubit. *Phys. Rev. A* **76**, 052314 (2007). doi:10.1103/PhysRevA.76.052314

29. G. Tóth, C. Knapp, O. Gühne, H. J. Briegel, Optimal spin squeezing inequalities detect bound entanglement in spin models. *Phys. Rev. Lett.* **99**, 250405 (2007). Medline doi:10.1103/PhysRevLett.99.250405

30. E. E. Edwards, S. Korenblit, K. Kim, R. Islam, M.-S. Chang, J. K. Freericks, G.-D. Lin, L.-M. Duan, C. Monroe, Quantum simulation and phase diagram of the transverse-field Ising model with three atomic spins. *Phys. Rev. B* **82**, 060412 (2010). doi:10.1103/PhysRevB.82.060412

31. B. Yoshimura, W. C. Campbell, J. K. Freericks, Diabatic ramping spectroscopy of many-body excited states for trapped-ion quantum simulators (2014). http://arxiv.org/abs/1402.7357

32. R. R. Ernst, G. Bodehausen, A. Wokaun, *Principles of Nuclear Magnetic Resonance in One and Two Dimensions* (Clarendon Press, Oxford, 1987).

33. A. Sørensen, K. Molmer, Entanglement and quantum computation with ions in thermal motion. *Phys. Rev. A* **62**, 022311 (2000). doi:10.1103/PhysRevA.62.022311

34. D. F. V. James, Quantum dynamics of cold trapped ions with application to quantum computation. *Appl. Phys. B* **66**, 181–190 (1998). doi:10.1007/s003400050373

35. C. Shen, L.-M. Duan, Correcting detection errors in quantum state engineering through data processing. *New J. Phys.* **14**, 053053 (2012). doi:10.1088/1367-2630/14/5/053053